Magnetic structures of $GdMn_6Ge_6$ - a nuclear magnetic resonance analysis

2000 J. Phys.: Condens. Matter 12 1065

(http://iopscience.iop.org/0953-8984/12/6/324)

J. Phys.: Condens. Matter **12** (2000) 1065–1084. Printed in the UK PII: S0953-8984(00)05955-5

Magnetic structures of $GdMn_6Ge_6$—a nuclear magnetic resonance analysis

P Rösch†, M T Kelemen†, E Dormann†, G Tomka‡ and P C Riedi‡

† Physikalisches Institut, Universität Karlsruhe, D-76128 Karlsruhe, Germany
‡ School of Physics and Astronomy, University of St Andrews, North Haugh, St Andrews, Fife KY16 9SS, UK

Received 12 June 1999, in final form 7 October 1999

Abstract. The origin of the interesting magnetic properties of $GdMn_6Ge_6$ in the low-temperature, low-field phase is a spiral arrangement of the magnetic moments. This has been established by pulsed nuclear magnetic resonance experiments. Spin-echo spectra taken in an external magnetic field, and the observed enhancement of the radio-frequency field, suggest the presence of a spiral structure. This information is crucial for a quantitative analysis of the complicated ^{55}Mn spectra. The anisotropy of the hyperfine field at the ^{55}Mn site is about 10% and the enhancement has been found to be highly anisotropic, as well. Comparing the temperature dependencies of the Zeeman splitting at the individual lattice sites, Mn has been identified as the source of the transferred hyperfine fields at the ^{73}Ge nuclei. An analysis of the ^{73}Ge and $^{155/157}$Gd spectra yields the size and relative orientation of the hyperfine fields and electric field gradients at the nuclei in agreement with ^{155}Gd Mössbauer spectroscopy results.

1. Introduction

Intermetallic compounds containing rare-earth elements (R) and manganese (Mn) have attracted considerable attention due to their complicated magnetic phase diagrams. An investigation of these properties can yield insight into the interplay between 3d and 4f magnetism. Most RMn_6Ge_6 compounds including $GdMn_6Ge_6$ and YMn_6Ge_6 crystallize in the $HfFe_6Ge_6$ structure. The lattice is composed of alternating layers with the sequence

$$\cdots \text{Ge(III)–Ge(II)–Mn–R/Ge(I)–Mn–Ge(II)–Ge(III)} \cdots .$$

R and Ge sites possess axial symmetry in contrast to the orthorhombic Mn site [1]. The magnetic structure of many RMn_6Ge_6 compounds has been analysed by neutron scattering and spiral structures have been found [2]. Although Y does not carry a magnetic moment, a spiral structure in the low-temperature phase of YMn_6Ge_6 could be deduced from neutron diffraction data [3]. In order to investigate the correlation between 3d–4f exchange interaction and spiral structures, the behaviour of $GdMn_6Ge_6$ is of particular interest as the pure spin magnetism of Gd in its ground state results in a negligible crystal-field interaction. At high temperatures, paramagnetism is observed for $GdMn_6Ge_6$. The ferrimagnetic phase between about 220 and 450 K is characterized by a spontaneous magnetization of 5 μ_B per formula unit. Lowering the temperature of the sample results in a pronounced decrease of its magnetization [4]. The magnetic structure at low temperatures is the main issue addressed by the present study. The large absorption cross section of Gd for neutrons requires an alternative local probe. In this

0953-8984/00/061065+20$30.00

contribution it is shown that complicated magnetic structures may be deduced from NMR spectra taken under carefully controlled experimental conditions.

After a short summary of relevant experimental details in section 2 the new experimental results are presented in section 3. Previously reported ^{73}Ge spin-echo spectra [4] have been completed by temperature sweeps and measurements in external magnetic fields. The quantitative interpretation of the Gd spectra [5] could be refined by diagonalizing the Hamiltonian. An analysis of the complex ^{55}Mn spectra based on the parameters obtained from the ^{73}Ge and Gd spectra results in an anisotropy of the hyperfine field of 10% at the Mn nuclei. The particular dependence of the spectra on the RF pulse amplitude and the shape of the spectra taken in external magnetic fields strongly suggest the presence of spin spiral structures in the low-temperature, low-field phase. In order to guide the reader through the complex analysis, the discussion in section 4 is subdivided into six subsections, and several necessary, but rather specialized NMR details are transferred into an extended appendix section.

2. Experimental details

The preparation of the $GdMn_6Ge_6$ powder samples has been described previously [6]. Measurements at frequencies below 100 MHz have been taken with commercial Bruker spectrometers CXP 200 and MSL 300 at Karlsruhe. For higher frequencies, the automated swept frequency spectrometer at St Andrews [7] has been used. Mn relaxation measurements in the range 200 MHz to 250 MHz have been performed using a modified Bruker spectrometer at Karlsruhe. Due to the enhancement of the RF field in the magnetically ordered compound $GdMn_6Ge_6$, a tuned circuit is not necessary. Except for the $^{155/157}$Gd spectrum at 77 K, non-resonant coils with inner diameters of 5 mm, typical lengths of 10 mm and inductances of about 0.2 μH have been used. A single loop in the vicinity of the sample allowed for the application of standard calibration procedures [8]. The spectra have been taken using spin echoes. Longitudinal relaxation has been investigated with the stimulated echo pulse sequence [9]. All the measurements in zero field have been taken on powder samples sealed in glass tubes. For the measurements in external fields up to 7 T, about 50 mg of $GdMn_6Ge_6$ powder were mixed with glue in an external magnetic field at room temperature. The aligned sample remained in the field until the glue was completely hardened. Additional specific NMR details are given in appendix A.

3. Experimental results

3.1. ^{73}Ge NMR spectra

Zero-field spectra of the spin-9/2 nucleus ^{73}Ge in $GdMn_6Ge_6$ for $T = 4.2$ K and $T = 77$ K have been reported previously [4]. Considerable RF enhancement was observed and the contributions of the three inequivalent lattice sites could be separated. The spectra of the two lattice sites characterized by higher resonance frequencies have been recorded for temperatures up to 240 K. With rising temperature all resonances shift to lower frequencies. The dependence of the signal amplitude on the pulse amplitude B_1 can be used to separate resonances originating from nuclei in domains from wall signals [10]. Figure 1 shows the result for $GdMn_6Ge_6$ at 4.2 K with pulse lengths of 2 μs and 3 μs. Maximum signal intensity corresponds to a B_1 induction of 30–40 μT as could be established by measuring the amplitude of the pulse induced in a coupling loop [4]. The pronounced decrease of signal intensity on both sides of the maximum is characteristic for all resonances contributing to the zero-field spectrum of $GdMn_6Ge_6$. Although the shape of the curve is very similar to that of a typical wall signal,

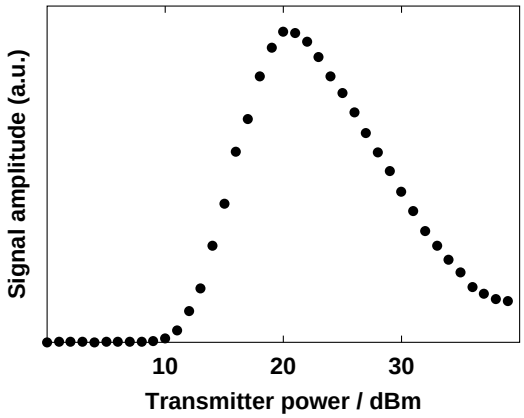

Figure 1. The area under the spin echo of the zero-field resonance of ^{73}Ge in $GdMn_6Ge_6$ (30.99 MHz) at 4.2 K as a function of transmitter power. Maximum signal intensity is observed for a power of 0.1 W corresponding to a B_1 flux density of 30–40 μT. (Pulse sequence (2 μs)–($\tau = 40$ μs)–(3 μs); see also appendix A.)

spectra obtained in external magnetic fields will show that the resonances do not originate from nuclei in domain walls.

If external magnetic fields up to about 1 T are applied, a splitting of the ^{73}Ge lines occurs. Maximum splitting is observed for an orientation of the external field parallel to the room temperature spontaneous magnetization, M_{ferri}. Figure 2 shows the spectra at 4.2 K taken for two orthogonal orientations of the samples. It should be noted that an external field with $B_{\text{ext}} = 0.3$ T oriented parallel to M_{ferri} yields the same splitting as $B_{\text{ext}} = 0.5$ T perpendicular to it. The application of external magnetic fields with inductions larger than 1 T results in a

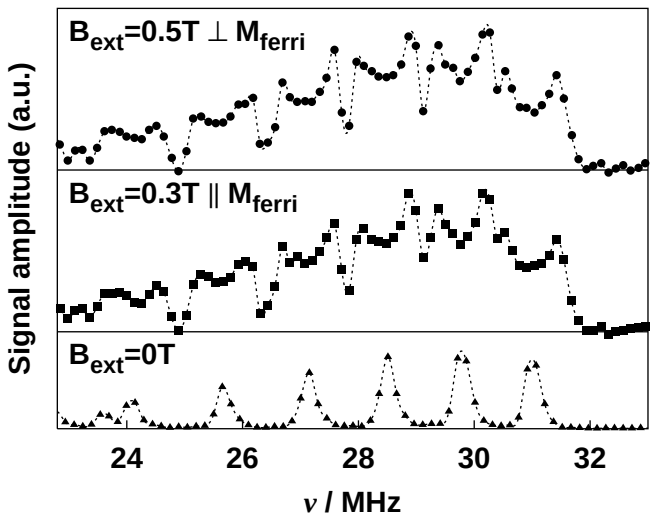

Figure 2. Splitting of the ^{73}Ge lines from the aligned $GdMn_6Ge_6$ sample at 4.2 K in external fields oriented parallel or perpendicular to the direction of the spontaneous magnetization in the ferrimagnetic phase, M_{ferri}. (Pulse sequence (2 μs)–($\tau = 100$ μs)–(2 μs), $B_1 \approx 50$ μT, uncalibrated.)

severe broadening of the lines and in a shift of the spectrum to lower frequencies (figure 3). Due to the fast relaxation and long receiver dead times, only the five lines with the highest resonance frequencies could be observed for $B_{\text{ext}} > 1$ T.

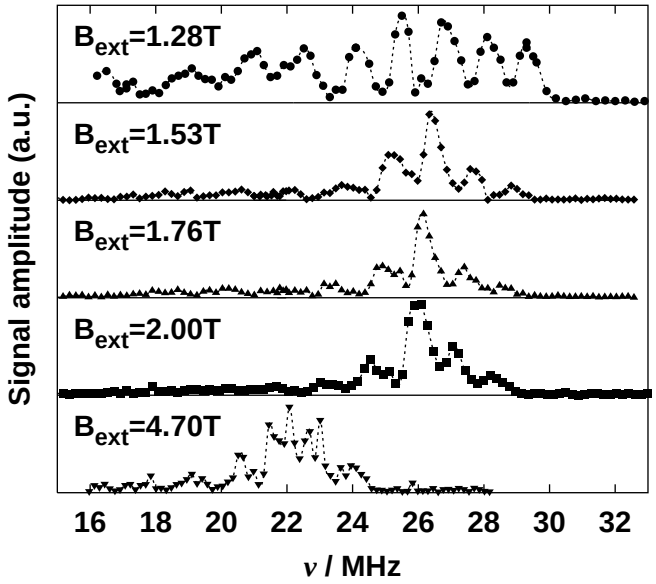

Figure 3. ^{73}Ge spectra of the oriented $GdMn_6Ge_6$ sample at 4.2 K in external magnetic fields oriented parallel to the spontaneous magnetization in the ferrimagnetic phase. (Pulse sequence (1.5 μs)–($\tau = 30$ μs)–(1.5 μs), $B_1 \approx 300$ μT, uncalibrated.)

3.2. $^{155/157}$Gd spectra

Four lines of the Gd zero-field spectrum of $GdMn_6Ge_6$ can be observed. The calibrated spectrum published in [5] is included in figure 4 for the convenience of the reader. Additional uncalibrated spectra were taken point by point in the temperature range 4.2–210 K. Short relaxation times and small signal intensity required 80 000 averaging steps for each data point of the spectrum shown in the upper part of figure 4. In order to avoid misinterpretations, the individual signals resulting from the averaging process were inspected. The centres of the intervals in which spin echoes could be identified are marked with filled triangles. At 4.2 K and pulse lengths of 3 μs, maximum signal strength was observed for a B_1 flux density of about 50 μT. The dependence of signal intensity on B_1 does not differ significantly from that observed for ^{73}Ge (figure 1).

3.3. ^{55}Mn spectra

In $GdMn_6Ge_6$ and YMn_6Ge_6 ^{55}Mn resonances could be detected in zero external field. NMR spectra are observed in the frequency intervals 200–250 MHz and 440–470 MHz [11]. Using a coil calibrated according to Lord and Riedi [7], a ratio of signal intensities $I(225\text{ MHz})/I(460\text{ MHz}) \approx 100$ at 4.2 K has been found for $GdMn_6Ge_6$. Similar enhancement factors were determined for the two frequencies (figure 5) indicating that the signal above 460 MHz (figure 6) originates from about one per cent of the ^{55}Mn nuclei present in the sample. Above 40 K, the resonances at the higher frequencies disappear, whereas the

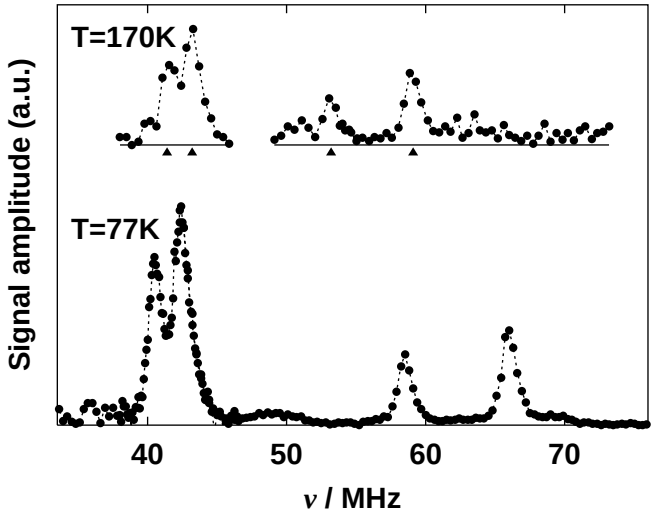

Figure 4. $^{155/157}$Gd zero-field spectra of $GdMn_6Ge_6$. ($T = 77$ K: tuned probe head, pulse sequence (0.6 μs)–($\tau = 35$ μs)–(0.9 μs). $T = 170$ K: $\tau = 11$ μs, 80 000 times of averaging per data point, no calibration. In the time domain, only in the intervals of about 1 MHz around the frequencies marked with filled triangles could spin echoes be observed. See also appendix A.)

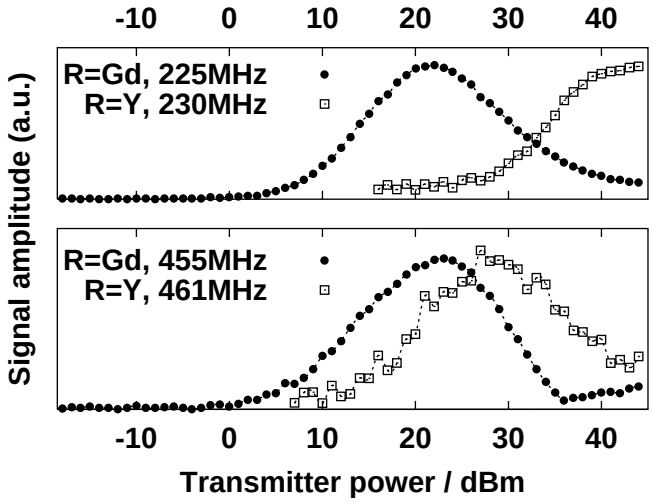

Figure 5. ^{55}Mn signal amplitude as a function of transmitter power for RMn_6Ge_6 at 4.2 K without an external magnetic field. Pulse sequence (1.5 μs)–(τ)–(3 μs) with $\tau = 10$ μs for R = Y and $\tau = 15$ (20) μs for R = Gd at 225 (455) MHz. 44 dBm corresponds to a linear RF field of $B_1 \approx 3$ mT. Thus, for R = Gd the largest signal amplitude is obtained for $B_1 \approx 300$ μT.

shape of the spectrum below 250 MHz does not change significantly. It can be shown that the resonances at the higher frequency originate from impurities (see appendix B).

In contrast to the zero-field ^{55}Mn spectrum in YMn_6Ge_6 shown in the upper part of figure 7 the $GdMn_6Ge_6$ sample exhibits a lineshape strongly depending on the amplitude of the rf pulse as can be seen from a comparison of the second curve of figure 7 (24 dBm) with the spectrum at the bottom of figure 14—see later (34 dBm). The latter is a superposition of two parts.

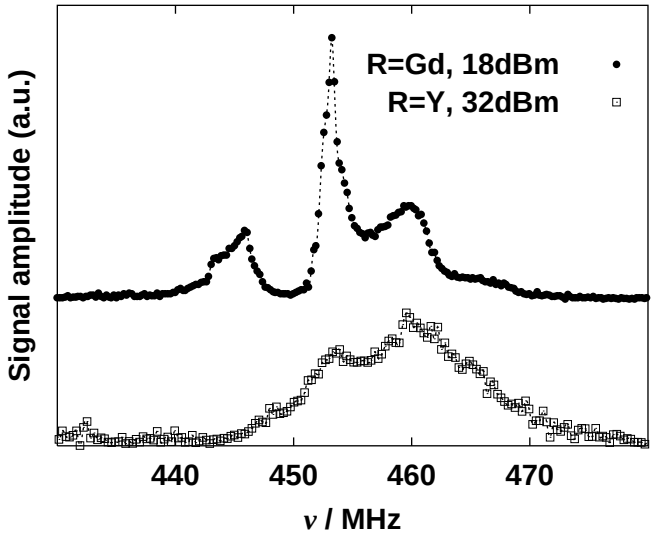

Figure 6. Calibrated ^{55}Mn zero-field spectra of RMn_6Ge_6 at 4.2 K above 400 MHz originating from an impurity phase. Untuned coil, pulse sequence (1.5 μs)–(τ = 12 μs)–(3 μs). See also appendix A and appendix B.

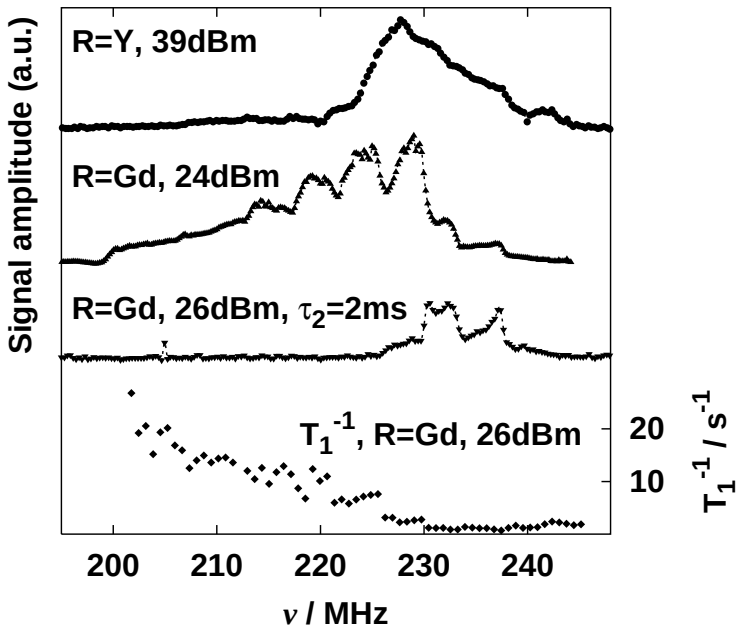

Figure 7. Calibrated ^{55}Mn spectra and the longitudinal relaxation rate of RMn_6Ge_6 (R = Y, Gd) at 4.2 K. Two curves at the top: the area under the spin echo, pulse sequence (1.5 μs)–(τ = 15 μs)–(3 μs). Third curve: the stimulated echo pulse sequence (3 μs)–(τ_1 = 15 μs)–(3 μs)–(τ_2)–(3 μs). Curve at the bottom: the longitudinal relaxation rate as a function of the frequency. See also appendix A.

Below 210 MHz one broad resonance has been observed, whereas the five equidistant lines constituting the part at higher frequencies could be resolved. If the pulse amplitude is reduced,

the spectrum broadens and the relative intensity of the contributions above 230 MHz increases (the curve labelled 24 dBm in figure 7). The latter is characterized by a relatively small longitudinal relaxation rate. In order to illustrate this, a spectrum from the T_1-measurement is shown. It should be noted that the signals with small enhancement factors show *larger* relaxation rates in contrast to a classical ferromagnet where the domain walls characterized by *large* enhancement factors exhibit fast relaxation [15]. The part of the $GdMn_6Ge_6$ ^{55}Mn spectrum with small relaxation rates covers the same frequency range as the ^{55}Mn spectrum of the YMn_6Ge_6 sample.

In order to obtain ^{55}Mn spectra in the ferrimagnetic phase of $GdMn_6Ge_6$, the rf coil containing the sample was re-calibrated at 273 K. Results for different pulse lengths are shown in figure 8. Both the lineshape and quadrupolar splitting observed for longer pulses at 273 K are identical to those of the Mn resonance at 4.2 K taken with large pulse power (see figure 14, later). Apparently, the shape of the spectrum at 273 K strongly depends on the B_1 flux density. Thus, a variation of pulse parameters is essential in order to separate the individual contributions to the spectrum. An analysis based on the lower part of figure 8 alone may give rise to misinterpretations as the seven lines seem to be equivalent.

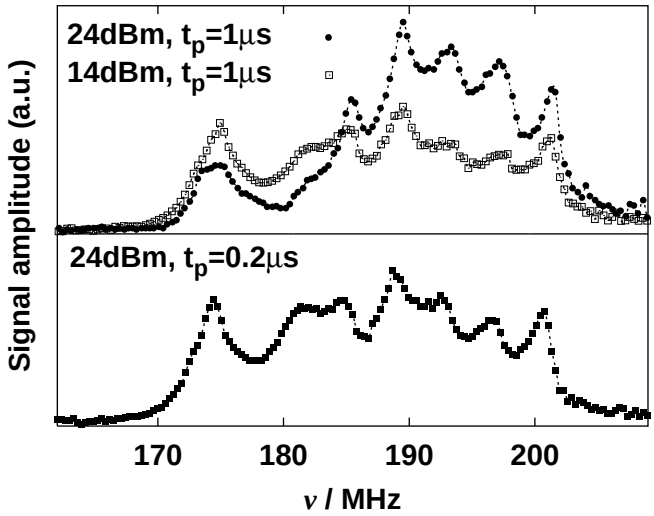

Figure 8. Calibrated ^{55}Mn spectra of $GdMn_6Ge_6$ at 273 K. Untuned coil, pulse sequences ($t_p = 1\ \mu$s)–($\tau = 9\ \mu$s)–(2 μs) and ($t_p = 0.2\ \mu$s)–($\tau = 5\ \mu$s)–(0.4 μs) for the top and bottom part respectively; see also appendix A.

The variation of signal amplitude with rf power for $GdMn_6Ge_6$ and YMn_6Ge_6 is shown in figure 5. The transmitter power corresponding to optimum signal amplitude, P_{opt}, for the signals below 300 MHz in $GdMn_6Ge_6$ is about one order of magnitude smaller than in YMn_6Ge_6 in contrast to the impurity signals around 450 MHz where P_{opt} is the same for the two samples within a factor of two. For $GdMn_6Ge_6$ the enhancement factor of the signal below 300 MHz in the low-temperature phase does not differ significantly from that in the ferrimagnetic phase. Assuming frequency-independent transmitter power and extrapolating the calibration done for ^{73}Ge, the B_1 flux density corresponding to maximum intensity of the ^{55}Mn signals in $GdMn_6Ge_6$ is found to be a factor of ten larger than for the ^{73}Ge and $^{155/157}$Gd signals at 4.2 K.

Measurements on $GdMn_6Ge_6$ in external magnetic fields have been performed at 4.2 K using bath cryostats in St Andrews. For flux densities up to 1.1 T, an electromagnet was used.

The sample coil was oriented parallel to the axes of the probe head allowing for a reorientation of the aligned powder sample by simply turning the coil. In order to compensate for the reduced enhancement factor compared to the zero-field measurement, the full transmitter power of 25 W has been applied without calibration. Figure 9 shows representative spectra for orientations of the external magnetic field parallel and perpendicular to the spontaneous magnetization in the ferrimagnetic phase. The most striking difference between the spectra concerns the relative amplitude of the resonance between 200 and 210 MHz. This line is far more prominent for $\boldsymbol{B}_{\text{ext}} \perp \boldsymbol{M}_{\text{ferri}}$. Between 0.3 and 0.5 T, the lineshapes for both orientations do not change considerably, but for $B_{\text{ext}} = 0.7$ T the peak at about 206 MHz has almost disappeared. Increasing the strength of the external field up to the limit of the electromagnet ($B_{\text{ext}} = 1.1$ T) results in a decrease of relative signal intensity in the range 220–230 MHz. The spectra referring to both orientations for $B_{\text{ext}} = 1.1$ T show a resonance at about 192 MHz that is more pronounced for $\boldsymbol{B}_{\text{ext}} \parallel \boldsymbol{M}_{\text{ferri}}$. The deviations of the profiles taken for $B_{\text{ext}} = 1.1$ T may be due to the fact that the transmitter power for $\boldsymbol{B}_{\text{ext}} \parallel \boldsymbol{M}_{\text{ferri}}$ was set to 20 dBm accidentally. A cryomagnet was used to investigate the shift of the ^{55}Mn resonances at flux densities up to 7 T at 4.2 K. With increasing strength of the external field the signal amplitude decreases and the presence of a spin echo needs to be verified for each frequency step. Nevertheless, the centre of the resonances could be determined without ambiguity even for $B_{\text{ext}} = 7$ T. The signals below and above 300 MHz both shift to lower frequencies with a rate of about 10 MHz T^{-1} characteristic for ^{55}Mn. A quantitative analysis is given in figure 15—see later.

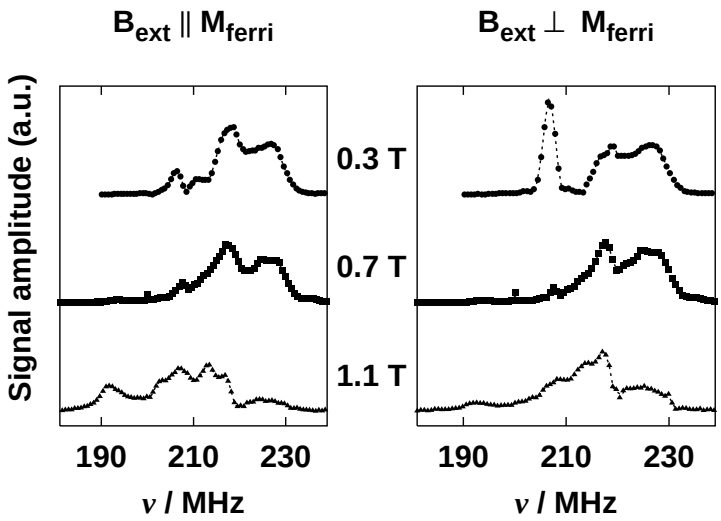

Figure 9. ^{55}Mn spectra of the oriented $GdMn_6Ge_6$ powder sample in external magnetic fields at 4.2 K. M_{ferri} denotes the direction of the spontaneous magnetization in the ferrimagnetic phase. (Pulse sequence (1 μs)–($\tau = 15$ μs)–(2 μs), normalized with respect to the area under the spectra, corrected for the frequency dependence of the receiver sensitivity (full transmitter power (25 W) without calibration).)

4. Discussion of the results

According to the relative weights of nuclear Zeeman and quadrupole interaction, NQR spectra are observed for $^{155/157}$Gd whereas the spectra of ^{73}Ge and ^{55}Mn are dominated by Zeeman splitting.

Ge does not carry a localized magnetic moment. The spectra of ^{73}Ge taken without an external magnetic field therefore reflect the hyperfine field transferred from Mn and Gd. The size and relative orientation of the hyperfine field and electric field gradient have already been determined [4]. Zero-field ^{73}Ge spectra of the two lattice sites with the largest hyperfine fields taken in the temperature range 4.2–220 K have been analysed according to the procedure described in [4]. Both the quadrupolar splitting and the orientation of the effective magnetic field at the nuclei perpendicular to the *c*-axis do not change significantly with temperature. Results are given in table 1; the average value of the angle between the *c*-axis and hyperfine field was found to be $(90 \pm 6)^\circ$. The Zeeman splitting definitely does change with temperature. Neutron scattering experiments on similar compounds have established magnetic structures based on ferrimagnetic building blocks consisting of two manganese layers and the Gd layer in between, and ferrimagnetic order has been deduced from magnetization measurements for the high-temperature phase of $GdMn_6Ge_6$. Both facts suggest ferrimagnetic spin waves as the mechanism responsible for the decrease of the hyperfine fields with increasing temperature. The temperature dependence of the Ge Zeeman frequency $^{73}\nu_z$ (the dotted line in figure 13—see later) is far less pronounced than that of Gd. It has been shown that $^{73}\nu_z(T)$ can be described by spin-wave theory in the full temperature range covered by figure 13, later [13]. As this model is only valid at temperatures well below the ordering temperature and the analysis of Gd hyperfine fields indicates a relative decrease of the Gd sublattice magnetization of at least 50 per cent in the temperature range 4.2 K–210 K, the hyperfine field at the Ge nuclei must be transferred from the Mn sublattice that is characterized by a considerably higher ordering temperature [4].

Table 1. Average quadrupole frequencies of the three Ge sites in $GdMn_6Ge_6$ for the temperature range 4.2 K–220 K. Due to the axial symmetry of the Ge sites the electric field gradient tensor is defined by its V_{zz}-component which has been calculated without shielding corrections.

	Ge(I)	Ge(II)	Ge(III)
ν_q/MHz	2.091 ± 0.004	3.183 ± 0.007	1.126 ± 0.008
$V_{zz}/10^{21}$ V m^{-2}	10.92 ± 0.02	16.23 ± 0.04	5.88 ± 0.04

4.1. Indications of spiral structure from low-field ^{73}Ge NMR

The splitting of the ^{73}Ge lines in small external magnetic fields suggests the presence of spiral structures in the low-temperature, low-field phase of $GdMn_6Ge_6$. First of all, it should be noted that although this phase is characterized by an almost vanishing spontaneous magnetization [4] considerable rf enhancement ($\eta_{rf} \approx 1000$) has been observed [4]. This is not consistent with simple antiferromagnetic order. The linear increase of sample magnetization with the strength of the external field reported in [13] is typical for a spin flop or a flat-spiral arrangement of magnetic moments. Assuming a flat-spiral arrangement and an external field vector applied perpendicular to the spiral axis, the splitting of the ^{73}Ge lines can be described in a quite straightforward way. See appendix C for details of the model.

The resonance frequencies of the individual transitions for ^{73}Ge are given by equation (9) in [4] derived from the expression given in [14]. For the simulation presented in figure 10, the gyromagnetic ratio of ^{73}Ge, $^{73}\gamma/(2\pi) = 1.49$ MHz T^{-1}, the susceptibility determined from magnetization measurements $\chi(4.2\text{ K}) = (1.9 \pm 0.2)\ \mu_B$ T^{-1}, $g = 2$ and $\phi_0 = 0$ have been used. For $kq \neq \pi$ with an integer number k, the value of q does not influence the averaging process. In order to approximate the orientation dependence of the rf enhancement, the anisotropy field of $B_{an} \approx 0.7$ T that has been determined via magnetization measurements

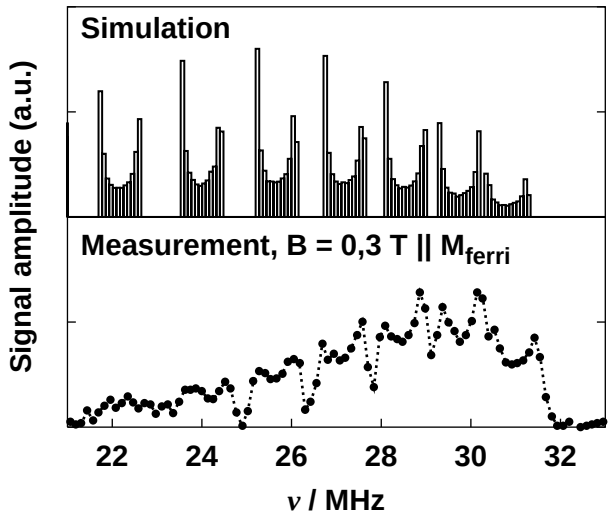

Figure 10. Simulated and experimental (uncalibrated) spectra of ^{73}Ge(II) in an external field of 0.3 T at 4.2 K for external field parallel to the magnetization in the ferrimagnetic phase. (Below $\nu = 25$ MHz the lines could not be resolved due to the overlapping ^{73}Ge(I) spectrum.)

is used. It is assumed that for $B_{\text{ext}} < B_{\text{an}}$ only the component of the external field parallel (or anti-parallel) to the anisotropy field affects the rf enhancement. On the basis of the standard equation [15], the enhancement factor for the moment at position p_n is given by

$$\eta_{\text{rf},n} \approx \frac{B_{\text{hf}}}{B_{\text{ext}} \cos(\phi_n - \phi_0) + B_{\text{an}}}. \tag{1}$$

Varying ϕ in the equations (C.1)–(C.3) given in appendix C and calculating the resonance frequencies $\nu_{m\leftrightarrow m-1}$ for $-I + 1 < m \leqslant I$, a histogram has been obtained. The counts of the individual bins represent the fraction of nuclei with resonance frequencies in the corresponding interval. Effects resulting in line broadening have been neglected. Despite the simplicity of the model, the numerical simulation reproduces both the position and shape of the lines in the uncalibrated observed spectrum for Ge(II) in an external field of 0.3 T oriented perpendicular to the c-axis (figure 10). In conclusion, the observed spectra are consistent with the presence of a spin spiral structure in the low-temperature, low-field phase of $GdMn_6Ge_6$.

The reason for the dependence of the splitting on the orientation of the aligned sample with respect to the external field shown in figure 2 is the polycrystalline nature of the powder sample. Each grain consists of crystallites with different orientations. Thus, aligning powder in an external field favours orientations parallel to the external field. However, other orientations are still present. For the spectrum shown in the top part of figure 2 the condition $\boldsymbol{B}_{\text{ext}} \parallel \boldsymbol{M}_{\text{ferri}}$ is met for a smaller percentage of crystallites than for the spectrum in the centre. The effect of the external field in terms of average line splitting is largest for an orientation $\boldsymbol{B}_{\text{ext}} \parallel \boldsymbol{M}_{\text{ferri}}$. It follows that the orientation dependence of the splitting is a direct consequence of the distribution of orientations resulting from the process of sample preparation.

4.2. High-field ^{73}Ge NMR

The spectra observed for an external field strength above 1 T (figure 3) can be analysed according to the method described in [4], as well. Setting the quadrupole splitting to the value given in table 1 and $\theta = 90^\circ$ yields the Zeeman frequencies plotted in figure 11. The Zeeman

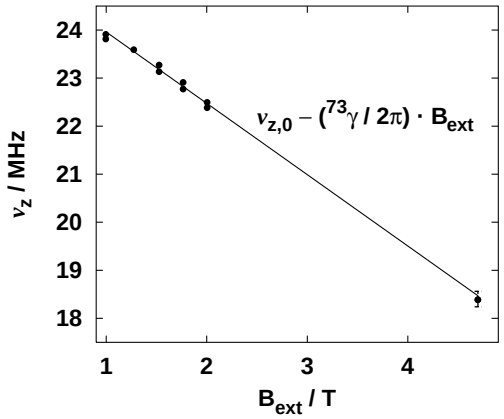

Figure 11. The Zeeman frequency of the ^{73}Ge(II) resonance of the oriented $GdMn_6Ge_6$ powder sample at 4.2 K in external fields oriented parallel to the spontaneous magnetization in the ferrimagnetic phase. The slope of the solid line is characteristic for ^{73}Ge; the parameter $\nu_{z,0}$ has been determined as 25.44 MHz.

frequencies change with a rate corresponding to the gyromagnetic ratio of ^{73}Ge and the offset determined by a least-squares fit is 25.44 MHz. This value is larger by about 400 kHz than the value determined in zero field at the same temperature [4]. One possible explanation for this observation is a slight rearrangement of the Mn moments under the influence of the external field. Assuming an angle of $\phi_{Mn} = 30^\circ$ between adjacent layers of the spiral as determined for $TbMn_6Ge_6$ [2], a change of 2° is sufficient to explain the observed frequency offset.

4.3. Unravelling of the $^{155/157}$Gd NQR spectra

The $^{155/157}$Gd spectra (figure 4) are dominated by quadrupolar interactions [5], but complicated because the condition $\nu_z \ll \nu_q$ is not strictly fulfilled as $\nu_q/\nu_z \approx 5$. Thus, for a quantitative understanding of the dependence of ν_z and ν_q on temperature, a more detailed analysis is required as elucidated in appendix D.

Equations (D.5) of appendix D have been solved for $^{155}\nu_1$, $^{157}\nu_1$, $^{155}\nu_2$ and $^{157}\nu_2$ observed for the temperature range 4.2 K–210 K. Figure 12 shows the resulting values for ν_q and ν_z. The quadrupolar splitting remains constant within experimental error indicating that the magnetically induced contribution to the electric field gradient at the Gd site is less than one per cent. In contrast, the Zeeman frequencies significantly decrease with rising temperature (see section 4.4). The average ratio $^{157}\nu_z/^{155}\nu_z = 1.330 \pm 0.005$ determined from the values shown in figure 12 is in good agreement to the value $^{157}\gamma/^{155}\gamma = 1.3122 \pm 0.0003$ found for $GdAl_2$ [16]. The ratio $^{157}\nu_q/^{155}\nu_q = 1.059 \pm 0.001$ differs by less than one per cent from the result $^{157}Q/^{155}Q = 1.065\,343(3)$ published in [17]. Finally, for $T = 4.2$ K the Zeeman and quadrupolar splitting are consistent with values derived from Mößbauer experiments [18] given in table 2. Thus, the assumption that $\theta = 90^\circ$ is supported not only by NQR measurements, but also by Mößbauer spectroscopy. Wall signals are not enhanced in Mößbauer spectroscopy. Thus, the parameters derived from the data correspond to the bulk material, and the agreement between Mößbauer spectroscopy and NQR indicates that the NQR spectra do not originate from domain walls.

In order to check whether the signal intensities measured at $T = 77$K are consistent with the interpretation presented above, the sum of four Gaussian functions has been fitted to

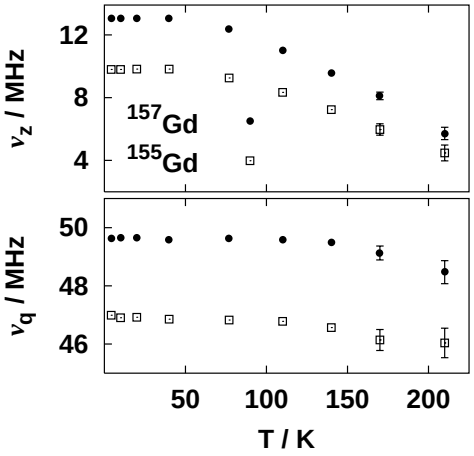

Figure 12. Zeeman and quadrupole frequencies for $^{155/157}$Gd calculated from the measured transition frequencies in zero field. See also appendix D.

Table 2. Comparison of ^{155}Gd NQR and Mößbauer spectroscopy results for $GdMn_6Ge_6$ at 4.2 K. The Mößbauer data [18] have been converted to frequencies using $^{155}Q = 1.30 \times 10^{-28}$ m^{-2} and $^{155}\gamma/(2\pi) = 1.307$ MHz T^{-1}.

^{155}Gd	ν_z/MHz	ν_q/MHz	θ
NQR	9.8 ± 0.2	47.0 ± 0.2	90°
Mößbauer spectroscopy	9.7 ± 0.7	53 ± 5	90°

the spectrum shown in figure 4. This procedure allowed for a separation of the double line around 42 MHz. The amplitudes of the Gaussian functions, A_{measured}, are given in table 3. They had to be corrected as explained in appendix E. The relaxation rates and corrected signal amplitudes are given in table 3. For both sets of lines, the intensity scales with the ratio of the gyromagnetic ratios (1.3) giving further evidence for the success of the calibration procedure and the interpretation presented.

Table 3. Intensities of $^{155/157}$Gd NQR signals in $GdMn_6Ge_6$ at 77 K normalized to the intensity of the line at 58.6 MHz. The transverse relaxation rates have been determined varying τ in the pulse sequence (0.6 μs)–(τ)–(0.87 μs) and fitting a single exponential to the measured echo amplitudes $I(\tau)$. For correction of the amplitude, see appendix E.

Isotope	^{155}Gd	^{157}Gd	^{155}Gd	^{157}Gd
ν_{res}/MHz	40.59 ± 0.02	42.44 ± 0.02	58.58 ± 0.02	66.09 ± 0.01
R/ms^{-1}	1.41 ± 0.02	1.85 ± 0.02	1.50 ± 0.02	2.45 ± 0.2
A_{measured}	2.4	3.3	1	1.4
$A_{\text{corrected}}$	3.5	$4.6 = 1.3 \times 3.5$	1	1.3

4.4. Temperature dependence of the Gd hyperfine field

The Zeeman splitting $^{157/155}\nu_z(T)$ (top part of figure 12) normalized to the maximum value $^{157/155}\nu_{z,\max}$ is plotted in figure 13 versus temperature. Assuming that $\nu_z(T)$ is proportional to the magnetization of the Gd sublattice and approximating the sublattice magnetization by the

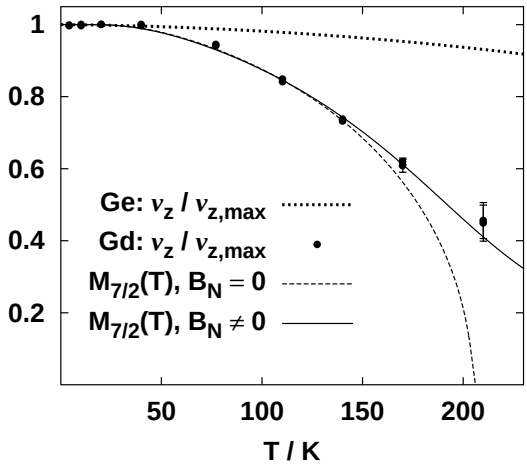

Figure 13. Zeeman frequencies of $^{155/157}$Gd in $GdMn_6Ge_6$ normalized to their maximum values as a function of temperature. The dotted line showing a relatively small variation with temperature represents the Zeeman frequency of ^{73}Ge(II). The broken line is the result from mean-field theory for a ferromagnetically coupled spin-7/2 system neglecting the hyperfine field induced by the Mn neighbours, B_N. The full line has been obtained by treating the hyperfine field induced by the Mn sublattice like an external field that shows the same temperature dependence as the Zeeman frequency of ^{73}Ge(II). Details are given in the text.

magnetization of a simple ferromagnet in zero external field obtained by mean-field theory, the curve denoted $M_{7/2}(T)$, $B_N = 0$ has been fitted to the data. According to this description, the spontaneous magnetization disappears at a temperature $T_{\mathrm{MF}} \approx 205$ K. This temperature coincides with the pronounced step of the $GdMn_6Ge_6$ magnetization curve which corresponds to the transition between the flat spiral and the ferrimagnetic spin arrangement [13]. Using the relation between T_{MF} and the effective exchange constant $J_{\mathrm{eff}}^{\mathrm{Gd}}$

$$T_{\mathrm{MF}} \approx \frac{S^{\mathrm{Gd}}(S^{\mathrm{Gd}}+1)}{3k_B} J_{\mathrm{eff}}^{\mathrm{Gd}} \tag{2}$$

with $S^{\mathrm{Gd}} = 7/2$ yields $J_{\mathrm{eff}}^{\mathrm{Gd}} \approx 40$ K. This value is of the same order of magnitude as the exchange constant deduced from magnetization measurements [13].

Figure 13 indicates that this simple model does not hold for temperatures above 140 K. This is not surprising as the spontaneous magnetization of the Gd sublattice is not the only contribution to the Gd hyperfine field. A more realistic description needs to include the hyperfine field transferred from the Mn atoms. In a first-order analysis this field is treated in analogy to an external magnetic field in the context of mean-field theory. Under the simplifying assumption that the transferred field, B_N, is oriented parallel to the hyperfine field resulting from the magnetization of the Gd sublattice and assuming that the temperature dependence of the transferred field is determined by spin-wave parameters similar to those reflected in the Ge hyperfine field, a least-squares fit has been performed. It yields a transferred hyperfine field corresponding to a flux density of 3.3 T (figure 13).

4.5. Anisotropy of ^{55}Mn electric quadrupolar and magnetic hyperfine interaction

Due to the orthorhombic symmetry of the Mn site in RMn_6Ge_6 the magnitudes of both the effective magnetic field and the electric field gradient depend on the orientation of the Mn moment with respect to the lattice. Thus, the ^{55}Mn lineshapes are more complex than that of

^{73}Ge and $^{155/157}$Gd. A quantitative analysis of ^{55}Mn spectra taken in the ferrimagnetic phase of $GdMn_6Ge_6$ at 273 K yields hyperfine parameters that can be used to analyse the spectra taken at 4.2 K. The discussion of the ^{55}Mn spectra gives further evidence for a spiral spin structure in the low-temperature, low-field phase.

The quantitative interpretation of the ^{55}Mn spectra is based on the equation for the transition frequencies given in [14]. ^{55}Mn spectra taken at 273 K (figure 8) can be divided in two parts by varying the B_1 flux density. In the frequency range 185–205 MHz five equidistant lines with a splitting of 4 MHz have been observed. Using $I = 5/2$, $\nu_q \approx 5$ MHz, $\nu_z \approx 200$ MHz and the equation mentioned above, it can be shown that the maximum shift resulting from the term proportional to ν_q^2/ν_z is smaller than 80 kHz which is considerably smaller than the width of the ^{55}Mn lines. Thus, the relation simplifies to

$$\nu_{m,m-1} = \nu_z \pm \frac{\nu_q}{2}\left(m - \frac{1}{2}\right)\left[(3\cos^2\theta - 1) - \eta\sin^2\theta\cos 2\phi\right] \qquad \nu_z = \nu_z(\theta, \phi). \tag{3}$$

At low temperatures, $\theta = 90^\circ$ has been found for all Ge sites and for the Gd site. As the position of the Ge(II) site ($c = 1/6$) is not symmetric with respect to the Mn layers ($c = \pm 1/4$), the contributions of antiferromagnetically aligned components of the Mn moment in the c-direction would not cancel each other at the Ge(II) site and the finding $\theta = 90^\circ$ for Ge(II) requires $\theta = 90^\circ$ for Mn in the low-temperature phase. In order to determine the orientation of the Mn moment with respect to the c-axis in the ferrimagnetic phase, a spectrum taken at 273 K is compared to the spectrum taken at 4.2 K with large pulse power (figure 14). From the fact that not only the profiles but also the splittings of the high-frequency parts of both spectra agree, it follows that $\theta = 90^\circ$ holds for the ferrimagnetic phase of $GdMn_6Ge_6$, as well. An x-ray diffraction study of the oriented powder sample of $GdMn_6Ge_6$ at room temperature indicates that most of the crystallites are oriented with their c-axes perpendicular to the direction of the spontaneous magnetization of $GdMn_6Ge_6$ in the ferrimagnetic phase. This supports the result of the NMR experiments. Using $\theta = 90^\circ$, the equations (3) and (C.1) can be simplified:

$$\begin{aligned} \nu_{m,m-1} &= \nu_z(\phi) \mp \frac{\nu_q}{2}\left(m - \frac{1}{2}\right)[1 + \eta\cos 2\phi] \\ \nu_z(\phi) &= [^{55}\gamma/(2\pi)]\sqrt{(B_{\text{eff}}^X\cos\phi)^2 + (B_{\text{eff}}^Y\sin\phi)^2}. \end{aligned} \tag{4}$$

In the low-temperature, low-field phase of $GdMn_6Ge_6$, a flat-spiral structure has been deduced from the ^{73}Ge spectra. Thus, all orientations of the magnetization with respect to the a-axis are present. As the spectrum shown in the lower part of figure 14 has been taken with a large rf pulse amplitude, its shape is determined by the Mn nuclei characterized by a relatively small enhancement factor. Taking into account the agreement of the profiles of the two spectra shown in figure 14 and the fact that for both temperatures $\theta = 90^\circ$ holds, the two distinct parts of the spectra most probably correspond to orientations of the Mn moment in the a–b plane characterized by maximum and minimum quadrupolar splitting or $\phi = 0^\circ$ and $\phi = 90^\circ$ in (4), respectively. For the spectrum taken at 273 K, the half-height full width of the resonance around 175 MHz is 4 ± 0.5 MHz and that of the broader line above 180 MHz is found to be 18 ± 0.5 MHz. Thus, comparing the ratios of experimental and theoretical linewidths allows the determination of the asymmetry parameter η (the same value has been determined for the spectrum taken at 4.2 K):

$$\frac{(18 \pm 0.5)\text{ MHz}}{(4.0 \pm 0.5)\text{ MHz}} = \frac{1+\eta}{1-\eta} \rightarrow \eta = 0.6 \pm 0.1.$$

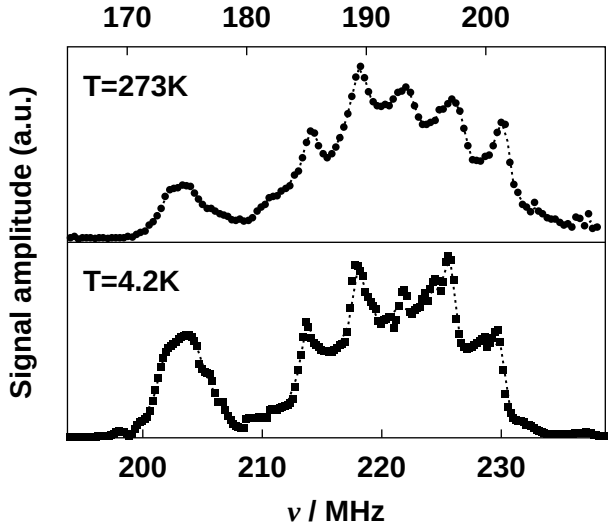

Figure 14. Comparison of calibrated zero-field ^{55}Mn spectra of $GdMn_6Ge_6$ at 4.2 K and 273 K with shifted origins of the frequency axes. Pulse sequences (1 μs)–(τ = 9 μs)–(1 μs) (top) and (1.5 μs)–(τ = 15 μs)–(3 μs) (bottom); transmitter power 24 dBm (top) and 34 dBm (bottom).

The observed splitting in the high-frequency part of both spectra ($\phi = 0^\circ$) is (4.0 ± 0.05) MHz. Using the asymmetry parameter determined above, the ^{55}Mn quadrupolar splitting can be obtained:

$$\nu_q = \frac{2 \times (4.0 \pm 0.05)\ \text{MHz}}{1 + \eta} \rightarrow \nu_q = (5.0 \pm 0.3)\ \text{MHz}.$$

Finally, the anisotropies of the hyperfine fields in the *a–b* plane are accessible via the centres of the higher- and lower-frequency parts of both spectra:

$$\frac{B^X_{\text{eff}}}{B^Y_{\text{eff}}} = \frac{\nu_z(\phi = 0^\circ)}{\nu_z(\phi = 90^\circ)} = \left(\frac{193.7\ \text{MHz}}{175\ \text{MHz}}\right)_{T=273\,\text{K}} = 1.11 \approx \left(\frac{221.8\ \text{MHz}}{203\ \text{MHz}}\right)_{T=4.2\,\text{K}} = 1.09.$$

4.6. Field dependence of ^{55}Mn spectra

The influence of external fields on the ^{55}Mn spectra of $GdMn_6Ge_6$ depends on the field strength. Applying external fields with flux densities above 1 T to the aligned powder sample of $GdMn_6Ge_6$ results in a shift of the ^{55}Mn spectra to lower frequencies with a rate corresponding to the gyromagnetic ratio of ^{55}Mn (figure 15). For $B_{\text{ext}} \leqslant 0.7$ T, the observed lineshape is considerably affected by the orientation of the aligned powder sample relative to the direction of the applied field (figure 9). Varying the pulse separation in both orientations, it could be shown that a dependence of the relaxation rates on sample orientation cannot explain this effect [21]. An interpretation based on the particularities of the rf enhancement for a spiral spin arrangement can be given: an external field oriented parallel to a magnetic moment has the same effect as an increased anisotropy field and results in a reduced rf enhancement [15]. If a spiral structure is present, the rf enhancement of the moments oriented parallel to the external field is affected most. The intensity of the line at about 205 MHz is significantly smaller for $\boldsymbol{B}_{\text{ext}} \parallel \boldsymbol{M}_{\text{ferri}}$ indicating that the moments possessing this resonance frequency are oriented parallel to both the external field and $\boldsymbol{M}_{\text{ferri}}$. According to figure 14, the line at 205 MHz in the low-temperature phase corresponds to the resonance at 175 MHz in the ferrimagnetic

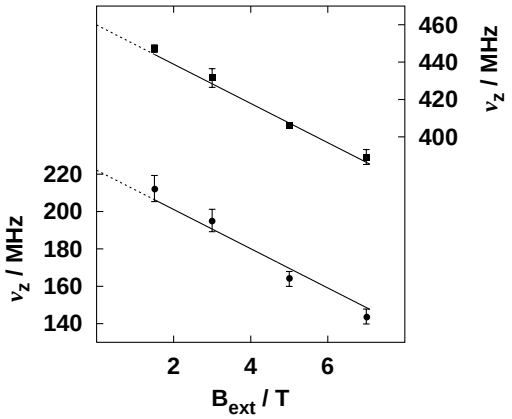

Figure 15. Centres of gravity of ^{55}Mn spectra of the oriented $GdMn_6Ge_6$ powder sample at 4.2 K in external magnetic fields up to 7 T oriented parallel to the spontaneous magnetization in the ferrimagnetic phase. The slopes of the lines correspond to the gyromagnetic ratio of ^{55}Mn.

phase. It follows, that the orientation of the majority of Mn moments in the ferrimagnetic phase coincides with the direction characterized by minimum quadrupolar splitting ($\phi = 90^\circ$ in equation (4)).

5. Concluding remarks

An analysis of NMR and NQR spectra of $GdMn_6Ge_6$ taken under different experimental conditions yields conclusive information concerning the magnetic structure of this compound. In agreement with magnetization measurements, a flat-spiral spin structure has been derived for the low-temperature, low-field phase. The Mn sublattice could be identified as the origin of the transferred hyperfine fields at the Ge sites, whereas the temperature dependence of the hyperfine parameters of Gd indicates two contributions to the hyperfine field. Below its ordering temperature, the magnetization of the Gd sublattice dominates. At higher temperatures, only the hyperfine field transferred from the Mn sublattice remains. Using the results of the ^{73}Ge and $^{155/157}$Gd spectra, the more complicated ^{55}Mn spectra could be analysed quantitatively.

Acknowledgments

We thank K H J Buschow for the samples, C Sürgers for the x-ray analysis and the Deutsche Forschungsgemeinschaft for financial support.

Appendix A. Specific NMR details

- The notation (1 μs)–(τ = 15 μs)–(2 μs) denotes a spin-echo sequence with pulses of 1 μs and 2 μs duration separated by an interval of 15 μs. A typical pulse sequence for stimulated echo experiments is (2 μs)–($\tau_1 = 15$ μs)–(2 μs)–($\tau_2 = 2$ ms)–(2 μs). In order to determine the longitudinal relaxation rate, τ_2 is varied.
- In the low-frequency range, the signal intensity was generally obtained by integrating the Fourier transform of the second half of the spin echo, correcting for the frequency dependence of the spectrometer sensitivity as described in [4].

- In contrast to the ESR convention, transmitter powers rather than attenuator settings are given in dBm.
- Unless stated otherwise, broken lines in figures are not a theoretical fit but simply a guide to the eye.

Appendix B. Impurity ^{55}Mn signals

The ^{55}Mn (figure 6) spectra above 400 MHz almost certainly originate from impurities. This statement is based on the following experimental results:

- The amplitude of the signals observed in the frequency interval 440 MHz–460 MHz at 4.2 K is two orders of magnitude smaller than that of the resonances around 220 MHz. From the very similar enhancement reported in figure 5 it follows that only about one per cent of the ^{55}Mn nuclei contribute to the signal at the higher frequency.
- The shape of the lines above 400 MHz is almost independent of the orientation of an external magnetic field with respect to M_{ferri}.
- Increasing the temperature to about 40 K causes the signals above 400 MHz to disappear whereas the other resonances can still be observed at 273 K. As the vanishing of the high-frequency signal does not correspond to a distinct feature of the magnetization curve, it is very unlikely that these signals are correlated with the magnetization of the bulk material.
- Comparing the dependence of the signal intensity on the rf amplitude (figure 5) for $GdMn_6Ge_6$ and YMn_6Ge_6 shows that the rf enhancement for the signals below 400 MHz differs by one order of magnitude whereas the signals above 400 MHz show similar enhancement factors. In contrast to the behaviour of the signals at lower frequencies that is in agreement with the different magnetic structures of the two compounds, the similar enhancement at the higher frequency indicates that the source of these signals is the same in both $GdMn_6Ge_6$ and YMn_6Ge_6.
- Even small amounts of manganese compounds with lower ordering temperatures than RMn_6Ge_6 on the surface of the powder grains could be responsible for the signals above 400 MHz. Possible candidates are Ge_3Mn_5 ($\nu_{\text{res,zero field}} = 422$ MHz), $MnCO_3$ ($\nu_{\text{res,zero field}} = 300$–$650$ MHz, $T = 1.4$–20.4 K) and Mn_3O_4 ($\nu_{\text{res,zero field}} = 550$–$560$ MHz, $T = 4.2$ K) [20]. As the impurities may form a thin layer on the RMn_6Ge_6 surface, their ^{55}Mn resonances could be shifted in the frequency domain around 450 MHz.

Appendix C. Modelling of NMR spectra for spiral structure

The model is based on the following assumptions [12]:

- The position of the nth magnetic moment is denoted by p_n. These moments are oriented perpendicular to the spiral axis that coincides with the c-direction of the lattice.
- If no external field is applied, each magnetic moment is rotated by an angle q_0 with respect to the neighbouring moment. The rotation axis is identical with the c-direction of the lattice. Thus, the angle between the nth moment and the a-axis, ϕ_n, is given by $\phi_n = \phi_{n-1} + q_0$. It is assumed that the moment at the position p_0 is oriented along the a-axis.
- The anisotropy of the hyperfine field results in a dependence of the Zeeman frequency on the orientation of the magnetic moment with respect to the main axes of the hyperfine tensor. Given the diagonal values of the hyperfine tensor in its eigensystem, B^X_{eff}, B^Y_{eff} and B^Z_{eff}, and the orientation of the magnetic moment relative to the main axis of the tensor in

terms of the rotation angles θ and ϕ, the Zeeman frequency without an external field is given by

$$\nu_{z,ZF}(\theta,\phi) = \frac{\gamma}{2\pi}\sqrt{(B_{eff}^{X}\sin\theta\cos\phi)^2 + (B_{eff}^{Y}\sin\theta\sin\phi)^2 + (B_{eff}^{Z}\cos\theta)^2} \tag{C.1}$$

with ϕ denoting the in-plane angle between the a-axis and the magnetic moment and θ the angle between the moment and the c-axis of the lattice. The equation given above is required for a simulation of ^{55}Mn, whereas the Zeeman frequency of Ge does not depend on ϕ due to the axial symmetry of the Ge sites.

- The sign of the hyperfine field is known to be negative. Thus, the Zeeman frequency becomes *smaller* if an external field is oriented parallel to the magnetic moments.
- A magnetic field applied perpendicular to the c-axis causes a rearrangement of the magnetic moment as described in [12]:

$$\phi_n(B_{ext}) = \phi_0 + nq - \frac{2\chi}{\mu}B_{ext}\sin(nq) \qquad \mu = g\mu_0\mu_B \qquad (q - q_0) \propto B_{ext}^2. \tag{C.2}$$

  χ denotes the magnetic susceptibility per formula unit. For the present analysis, the g-factor is set to 2.0. The parameter q replaces the zero-field parameter q_0. Equation (C.2) basically says that with increasing magnitude of the external field, B_{ext}, orientations of magnetic moments parallel (and anti-parallel) to the external field become more and more likely.
- Finally, the hyperfine field at the nucleus of the nth atom for $\theta = 90^\circ$ can be found by combining (C.1) and (C.2). The external field vector is added to the zero-field contribution of the hyperfine field yielding

$$\nu_z(n, B_{ext}) = \sqrt{\nu_{z,ZF}^2(90^\circ,\phi_n) + \left(\frac{\gamma}{2\pi}B_{ext}\right)^2 - 2\nu_{z,ZF}(90^\circ,\phi_n)\frac{\gamma}{2\pi}B_{ext}\cos(\phi_n - \phi_0)}. \tag{C.3}$$

  It should be noted that (C.3) already contains the negative sign of the hyperfine field.

Appendix D. Analysis of $^{155/157}$Gd NQR spectra

Due to the dominance of the quadrupolar interaction it is convenient to transform the Zeeman Hamiltonian into the eigensystem of the electric field gradient tensor. Using $\nu_z = [\gamma/(2\pi)]|\vec{B}_{eff}|$ yields

$$\mathcal{H}_z = -2\pi\nu_z\left[\frac{1}{2}\sin\theta(\mathcal{I}_+e^{-i\phi} + \mathcal{I}_-e^{i\phi}) + \mathcal{I}_z\cos\theta\right] \tag{D.1}$$

where ϕ defines the orientation within the a–b plane of the lattice. Using the axial symmetry of the Gd site in $GdMn_6Ge_6$, the Hamiltonian describing the quadrupolar interaction is obtained:

$$\mathcal{H}_q = \frac{eQV_{zz}}{4I(2I-1)\hbar^2}(3\mathcal{I}_z{}^2 - \mathcal{I}^2). \tag{D.2}$$

For $I = 3/2$, the matrix representation of the Hamiltonian $\langle\frac{3}{2}m|\mathcal{H}_q + \mathcal{H}_z|\frac{3}{2}m'\rangle$ is

$$\mathcal{H} = \begin{bmatrix} -(h/2)\nu_q + \frac{3}{2}h\nu_zC & -\frac{\sqrt{3}}{2}h\nu_zSe^{i\phi} & 0 & 0 \\ -\frac{\sqrt{3}}{2}h\nu_zSe^{-i\phi} & (h/2)\nu_q + \frac{1}{2}h\nu_zC & -h\nu_zSe^{i\phi} & 0 \\ 0 & -h\nu_zSe^{-i\phi} & (h/2)\nu_q - \frac{1}{2}h\nu_zC & -\frac{\sqrt{3}}{2}h\nu_zSe^{i\phi} \\ 0 & 0 & -\frac{\sqrt{3}}{2}h\nu_zSe^{-i\phi} & -(h/2)\nu_q - \frac{3}{2}h\nu_zC \end{bmatrix} \tag{D.3}$$

(where C stands for $\cos\theta$ and S for $\sin\theta$). The angle ϕ does not influence the eigenvalues and can be set to zero. For $\theta = 90^\circ$ the Hamiltonian can be diagonalized analytically yielding four energy levels $E_1, \ldots, E_4$ corresponding to the eigenstates $|\Psi_1\rangle, \ldots, |\Psi_4\rangle$:

$$\begin{aligned} E_1/h &= -\frac{1}{2}\sqrt{3\nu_z^2 - 2\nu_z\nu_q + \nu_q^2} - \frac{1}{2}\nu_z \\ E_2/h &= +\frac{1}{2}\sqrt{3\nu_z^2 - 2\nu_z\nu_q + \nu_q^2} - \frac{1}{2}\nu_z \\ E_3/h &= -\frac{1}{2}\sqrt{3\nu_z^2 + 2\nu_z\nu_q + \nu_q^2} + \frac{1}{2}\nu_z \\ E_4/h &= +\frac{1}{2}\sqrt{3\nu_z^2 + 2\nu_z\nu_q + \nu_q^2} + \frac{1}{2}\nu_z. \end{aligned} \tag{D.4}$$

Using the approximate values for ν_z and ν_q published in [5] it turns out that the frequency corresponding to the difference between E_1 and E_3 is smaller than the linewidth observed. The eigenvectors of (D.3) allow for an estimation of the probabilities P of transitions between the eigenstates. For magnetic transitions and the approximate values for ν_q and ν_z it could be shown that

$$\begin{aligned} P(|\Psi_1\rangle \leftrightarrow |\Psi_4\rangle) &\approx P(|\Psi_3\rangle \leftrightarrow |\Psi_4\rangle) \\ P(|\Psi_1\rangle \leftrightarrow |\Psi_2\rangle) &\approx P(|\Psi_3\rangle \leftrightarrow |\Psi_2\rangle). \end{aligned}$$

It follows that the average of E_1 and E_3 can be used to calculate the two relevant transition frequencies ν_1 and ν_2:

$$\begin{aligned} \nu_1 &= \frac{E_4 - (E_1 + E_3)/2}{h} = \frac{3}{4}\sqrt{4\nu_z^2 + 2\nu_z\nu_q + \nu_q^2} + \frac{1}{4}\sqrt{4\nu_z^2 - 2\nu_z\nu_q + \nu_q^2} + \frac{1}{2}\nu_z \\ \nu_2 &= \frac{E_2 - (E_1 + E_3)/2}{h} = \frac{1}{4}\sqrt{4\nu_z^2 + 2\nu_z\nu_q + \nu_q^2} + \frac{3}{4}\sqrt{4\nu_z^2 - 2\nu_z\nu_q + \nu_q^2} - \frac{1}{2}\nu_z. \end{aligned} \tag{D.5}$$

The transition with the frequency $\nu = (E_4 - E_2)/h \approx 20$ MHz is allowed, as well. Due to the overlap with the much stronger ^{73}Ge signals, this resonance could not be observed. However, the presence of this signal may have disturbed the intensity calibration of the ^{73}Ge lines published in [4].

Appendix E. Correction of signal amplitudes

According to [19], the following relation holds for the maximum amplitude of the voltage induced in the rf coil during a spin echo if $\nu_q > \nu_z$:

$$U_{\text{coil}} \propto \frac{\gamma\nu_{\text{res}}^2}{T} e^{-2\tau R}. \tag{E.1}$$

R denotes the spin–spin relaxation rate, τ is the pulse separation and ν_{res} is the resonance frequency. The application of the calibration process [8] corrects for the influence of the induction law ($U_{\text{coil}} \propto \nu_{\text{res}}$) resulting in a linear relationship between signal amplitude and resonance frequency. For fixed temperature, the corrected signal amplitude for $\tau = 0$ can be calculated as follows:

$$A_{\text{corrected}} = \frac{A_{\text{measured}}}{\nu_{\text{res}}/1\ \text{MHz}} e^{2\tau R} \propto \gamma. \tag{E.2}$$

References

[1] Brabers J H V J, Duijn V H M, de Boer F R and Buschow K H J 1993 *J. Alloys Compounds* **198** 127
[2] Schobinger-Papamantellos P, Rodríguez-Carvajal J, André G and Buschow K H J 1995 *J. Magn. Magn. Mater.* **150** 311
[3] Venturini G, Welter R and Ressouche E 1993 *J. Alloys Compounds* **200** 51
[4] Rösch P, Kelemen M T, Pilawa B, Dormann E and Buschow K H J 1996 *J. Magn. Magn. Mater.* **164** 175
[5] Rösch P, Weizenecker J, Kelemen M T, Ruf J, Zobel C and Dormann E 1998 *J. Magn. Magn. Mater.* **177–181** 1071
[6] Dirken M W, Thiel R C, Brabers J H V J, de Boer F R and Buschow K H J 1991 *J. Alloys Compounds* **177** L11
[7] Lord J S and Riedi P C 1995 *Meas. Sci. Technol.* **6** 149
[8] Dormann E 1991 NMR in intermetallic compounds *Handbook on the Physics and Chemistry of Rare Earths* ed K A Gschneidner Jr and L Eyring (Amsterdam: North-Holland) p 63
[9] Hahn E L 1950 *Phys. Rev.* **80** 580
[10] Oliveira I S and Guimaraes A P 1997 *J. Magn. Magn. Mater.* **170** 277
[11] Rösch P, Dormann E, Tomka G and Riedi P C 1996 *28th Ampère Congr. (Canterbury, 1996)* ed M E Smith and J H Strange, extended abstracts p 490
[12] Nagamiya T, Nagata K and Kitano Y 1962 *Prog. Theor. Phys.* **27** 1253
[13] Kelemen M T, Rösch P and Dormann E 1998 *J. Magn. Magn. Mater.* **188** 195
[14] Carter G C, Bennett L H, Kahan D J 1977 Metallic shifts in NMR *Progress in Materials Science* Part I, vol 20, ed B Chalmers, J W Christian and T B Massalski (Oxford: Pergamon) p 79
[15] Turov E A and Petrov M P 1972 *Nuclear Magnetic Resonance in Ferro- and Antiferromagnets* (New York: Halstead)
[16] Dormann E, Dressel U, Kropp H and Buschow K H J 1984 *J. Magn. Magn. Mater.* **45** 207
[17] Unsworth P J 1969 *J. Phys. B: At. Mol. Phys.* **2** 122
[18] Mulder F M, Thiel R C, Brabers J H V, de Boer F R and Buschow K H J 1993 *J. Alloys Compounds* **190** L29
[19] Das T P and Hahn E L 1958 Nuclear quadrupole resonance spectroscopy *Solid State Physics* Supplement 1, ed F Seitz and D Turnbull (New York: Academic)
[20] Feldmann D, Kirchmayr H R, Schmolz A and Veliscescu M 1971 *IEEE Trans. Magn.* **7** 61
[21] Rösch P 1997 Analyse der magnetischen Eigenschaften von $GdMn_6Ge_6$ mittels Kernspinresonanz sowie Aufbau eines dafür geeigneten Spektrometers *Thesis* Physikalisches Institut, Universität (TH) Karlsruhe